Experiments in Fluids (2021) 62:56
https://doi.org/10.1007/s00348-021-03153-3

RESEARCH ARTICLE

Coalescence of sessile droplets driven by electric field in the jetting-based 3D printing framework

J. Plog[1] · Y. Jiang[1] · Y. Pan[1] · A. L. Yarin[1]

Received: 3 December 2020 / Revised: 12 January 2021 / Accepted: 20 January 2021 / Published online: 1 March 2021

Abstract

The recent developments revealed droplet jetting technologies, as applied to 3D printing (additive manufacturing), to be a strategic tool in creating biological sensors and wearable, flexible three-dimensional electronic devices. While the typical discretely formed droplets tend to limit throughput, several highlights to the jetting process include an ample choice of ink/substrate combinations and printing with nearly zero waste. From a functional manufacturing perspective, it is important to understand how these discretely formed droplets can be interconnected into digitally patterned lines and films within the limitations of the physics and hardware involved. Here, we investigate the effectiveness of a Coulomb force created by charged electrodes placed either below the substrate or on the printhead. From the physical point of view, the phenomenon of dynamic electrowetting-on-dielectric (DEWOD) is used. It is demonstrated that sessile droplets, placed initially separately with little chance of natural coalescence, can be selectively coerced by the added electric field into the electrically enhanced forced coalescence. Positive results were recorded for both electrode configurations at spacing distances greater than those achieved in literature. These results reveal novel manifestations of electrically driven coalescence, which hold great promise for new manufacturing design opportunities, reduction in raw material use, operation on extremely rough surfaces, and continuous narrow prints in situations where the previous approaches failed. In addition to droplet-into-line coalescence, the first-approximation potential to merge 2D droplet arrays into films is also demonstrated.

✉ Y. Pan
yayuepan@uic.edu

✉ A. L. Yarin
ayarin@uic.edu

[1] Department of Mechanical and Industrial Engineering, University of Illinois at Chicago, 842 W. Taylor St, Chicago, IL 60607-7022, USA

Graphic abstract

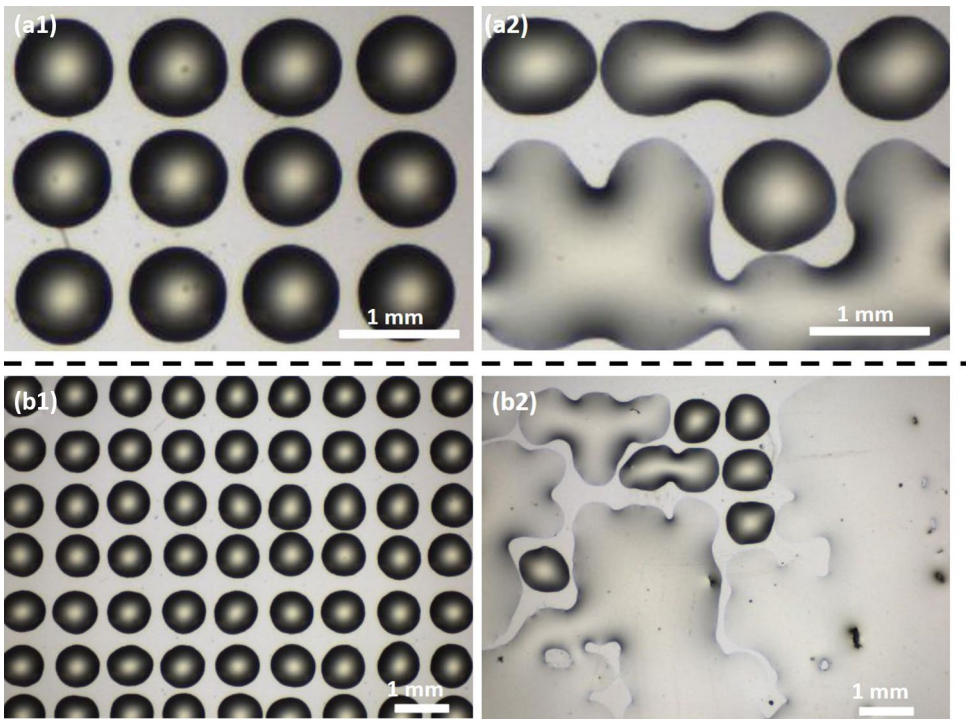

1 Introduction

Nearly 70 years since conception, inkjet printing has evolved into a staple within modern industry as a useful advanced fabrication tool. While relatively simple in principle, the trend to maximize DPI (dots per inch) while concurrently reducing the size of the machinery, has made the successful implementation of this non-contact process very complex. Despite these and other challenges, inkjet printing remains at the forefront as a direct printing technique when fabricating functional electronics (Matavž et al. 2018; Salaoru et al. 2019; Seipel et al. 2018; Vaithilingam et al. 2018), sensors and three-dimensional biological materials (Maddaus et al. 2016; Kumar et al. 2011). Because building structures pixel-by-pixel, and layer-by-layer requires placement of adjacently located droplets, the coalescence between two merging drops is one key dynamic phenomenon receiving attention in current research works (Soltman et al. 2010; Andrieu et al. 2002; Li et al. 2010; Castrejon et al. 2011; Stringer and Derby 2010; Gokhale et al. 2004; Boley et al. 2013). The majority of the above-mentioned works aimed at creating a continuous line or a conducting trace through coalescence. Applying electric forces (essentially, associated with the Maxwell stresses at the droplet surface) could cause electrocoalescence, which could be useful for droplet manipulation or potentially beneficial to manufacturing as a novel tool. While admittedly the coalescence of two adjacent droplets is not always desirable (Bhuvana et al. 2010; Boley et al. 2009), the ability to control or tune the phenomenon may prove advantageous.

Coalescence can occur relatively quickly in inkjet printing, with literature claiming the characteristic times of the order of ~100 ms or less (Sarojini et al. 2016). The characteristic hydrodynamic time of droplet coalescence is $\tau_H = \mu R_0/\sigma$. It reveals that the timescale related to the viscous regime of coalescence can be reduced by several orders of magnitude when the viscosity (μ) is relatively low and the surface tension (σ) is relatively high. Also worth mentioning is that the characteristic hydrodynamic time is proportional to droplet size (R_0), which continues to decrease as new, high-resolution techniques emerge. High-resolution inkjet patterns typically have features in the 10–100 μm range (Singh et al. 2010), but current trends are aiming for nanometer-sized pixels on both solid and flexible, porous and non-porous substrates. It is important to keep these ever-shrinking scales in mind when considering techniques used to manipulate functional, drop-on-demand inkjet printing, say, to enhance or prevent droplet coalescence on a substrate. Indeed, an additional external electric force applied to droplets should be capable of a greater switching frequency than

droplet formation frequency at the inkjet nozzle (~10 kHz) and/or the inverse hydrodynamic time τ_H^{-1} of the fluid. For the two inks of interest in the present work (linseed oil and Spot-E), the values of τ_H were found to be 1.2 ms and 0.3 ms, respectively, which yields τ_H^{-1} 833 Hz and 3333 Hz, respectively, which are well below the frequency at which the electric field (E.F.) can be adjusted. The latter makes application of the electric forces for droplet coalescence or splitting extremely attractive. If fact, frequencies up to one-trillion cycles/s (Samoska 2011), have been reported from modern amplifiers, which significantly exceeds the value of τ_H^{-1} in the present case. While this should not imply the ability to control droplets faster than their natural frequency, rather it shows the E.F. will be fully capable of controlling droplets as fast as they are created or their eigenfrequencies allow. Adding even more to the appeal, the previous work of this group has revealed the ability to retrofit existing machinery to produce enhanced prints without the need for a costly replacement (Plog et al. 2020a, b).

The E.F. application is one of several industrial trends aiming at manipulation and, essentially, control of manufacturing materials via sorting (Fidalgo et al. 2008), transporting (Cho et al. 2003), merging (Hung et al. 2006), splitting (Link et al. 2004), and storing droplets (Wang et al. 2009). In addition to the E.F. Lee et al. (2012, 2013) and Plog et al. (2019; 2020a, 2020b) used for dynamic electrowetting-on-dielectrics (DEWOD), forces resulting from acoustic waves, electro-magnetic excitation, as well as thermal and hydrodynamic phenomena-related forces can be employed (Franke et al. 2009; Zhao et al. 2009; Nguyen et al. 2007; Ozkan et al. 2003; Zeng et al. 2009). It should be emphasized that the present work uses only the E.F. generated by a DC source. Note also that AC voltages have been shown to stimulate the resonance frequencies of sessile droplets within a transverse E.F. to either coalesce or move such droplets through vibrations (Löwe et al. 2018).

Many works are directly related to functional inkjet printing, with several having experimental methods and theoretical explanations related to the interactions between adjacently placed droplets (Wu et al. 2012; Shimoda et al. 2003; De Gans et al. 2004). For calculations, Stringer and Derby (2010) used a simple conservation of volume model proposed by Duineveld (2003) to study the instability of an inkjet-printed line on a homogenous and flat substrate. While several authors explain printed stability in terms of a geometric model, Soltman et al. (2010) not only studied the overlapping of adjacent droplets into lines, but also overlapping of adjacent lines into thin films, and explained the observed morphologies. Although less popular, at least one method in functional inkjet printing avoids the occurrence of overlapping entirely. Boley et al. (2009) chose a two-pass approach where every other pixel is printed in the first pass allowing time to dry before going back over to fill in the gaps. While this method was able to produce uniform lines with a claimed beneficial thickness, it would limit the throughput as the printhead would be required to make at least two passes per trace. It should be emphasized that one benefit of the non-overlapping method proposed in the present work is the reduction of 'drawback' where the second (impacting) droplet is pulled in the direction of the first (sessile) droplet, which becomes exceedingly pronounced when the viscosity is low (Lee et al. 2012). The 'drawback' may unfavorably break, distort and/or budge a trace line. The reduction of this phenomenon through electrocoalescence, instead of traditional jetting overlap could be beneficial. As to our knowledge, not a single publication was found integrating electrocoalescence with droplet jetting-based 3D printing techniques, which is the main aim of the present work.

2 Experimental

A great benefit of inkjet printing is the broad range of working fluids which leads to a subsequent number of potential directions for research. Printable inks consist of three main components: carrier medium (water or another solvent) including colorant (pigment), additives (e.g., carbon nanotubes, etc.), and binder (resin) (Aydemir et al. 2010). In the present work, two working fluids were chosen based on their relevance to industry or research. Linseed and or soybean oil is the base for most inks and is considered a "green" (bio-renewable) vegetable base for inks. Linseed oil is also known to create prints with a high brightness value (Aydemir et al. 2018) and be a major component in functional resins (Koivula 2012). Synthetic polymers, which are critical in flexible electronics, can also add advantageous physical characteristics (e.g., flexibility, tunable conductivity, low weight, etc.) to ink formulations (Nardes et al. 2007). A pre-manufactured polymer ink, Spot-E (Spot-A materials) along with linseed oil (Amazon) were purchased for the present work. Relevant properties of these liquids, which are ionic conductors (Chang and Yeo 2010; Yarin et al. 2014), are listed in Table 1.

If two droplets of similar inks make contact, one anticipates coalescence driven by minimization of surface energy (Rayleigh 1896; Landau and Lifshitz 1987). Here, we experimentally demonstrate that droplets comprised of typical inkjet fluids can achieve line/film coalescence without direct overlap of sequentially printed droplets, which has never been achieved in the existing literature, as to our knowledge. Electrodes, with the ability to create an electric field strength of 1.57 kV/cm between them, were placed in two configurations. For an initial test, both electrodes are placed parallel on the surface (Fig. 1a), while the subsequent tests changed the configuration by placing the electrodes on the print head

Table 1 Properties of the inks used in the experiments

	Surface tension	Viscosity	Vapor pressure	Boiling temp.	Elec. cond.
Spot-E	33 mN/m	400 mPa × s	negligible	–	1.08×10^{-6} S/m
Linseed oil	40.4 mN/m	39 mPa × s	negligible	315 C	1.12×10^{-8} S/m

and perpendicular to the horizontal surface (Fig. 1b). When charged, these electrodes provide an additional Coulomb force to facilitate the formation of a line (droplet-to-droplet coalescence) or a film (line-to-line coalescence). Liquids are ionic conductors and charge re-distribution in them proceeds on the scale of the charge relaxation time τ_C, which is on the 1 µs–1 s time scale (Yarin et al. 2014). When the characteristic droplet evolution time τ_H is of the order of, or longer than the charge relaxation time, extra ions have enough time to migrate to the free surface toward the electrode with the opposite polarity (the leaky dielectric Melcher-Taylor model; Melcher and Taylor 1969; Russel et al. 1992; Saville 1997; Castellanos and Pérez 2007; Chang and Yeo 2010; Yarin et al. 2014). That means that liquid, essentially, behaves as a perfect conductor, in spite of its low electrical conductivity. The net electric charges created at the surface, thus interact with the nearby electrodes of the opposite polarity, which constitutes the action of additional Coulomb forces applied to the liquid from the electrodes.

Accordingly, droplets placed on a surface initially with no overlap can be stretched out of their lowest energy state (an almost spherical segment) and literally reach out to join with a neighboring droplet/droplets forming new energy states. It is important to note that the case displayed in Fig. 1a is less than ideal for real-world printing as the effects of the embedded electrodes would diminish as the build height increases. However, this configuration was initially chosen for ease of application and visualization through high-speed recording. In the second case tested (Fig. 1b), the electrodes are not limited to the build surface, having their effects consistent throughout the entire build.

The droplets used in the present experiments were of the order of 200 µm–1 mm (the volume-equivalent diameter). It should be emphasized that Plog et al. (2019) demonstrated that droplets of sizes 200 µm–3 mm could be manipulated and moved by the electric forces on a number of dielectric substrates at the electric field strengths well below the dielectric breakdown in air of ~ 30 kV/cm. Accordingly, the electric field strength of 1.57 kV/cm employed here is sufficient for manipulation of droplets of sizes relevant in the 3D printing, and there is a sufficient leverage for manipulation of even smaller droplets by safely increasing the electric field strength beyond the value of 1.57 kV/cm.

Experiments were performed with sessile droplets of the aforementioned liquids printed with an offset using a modified DIW (Direct Ink Writing) automated dispensing system utilizing D.O.D. (droplet-on-demand) generation. To generate droplets of diameter d ~ 1 mm, a commercial droplet generator (Nordson Ultimus I) was utilized along with a 32-gauge needle (109 µm inner diameter). The droplet generator creates a well-defined pressure pulse for a specific time interval driving the ink through a blunt needle at a pressure ranging from 0.1 to 70 psi. With the printing needle positioned ~5 mm above the substrate, the droplet impact velocities were estimated to be ~ 0.31 m/s. This process is carried out by depositing the first droplet followed by a translation of the chosen substrate before a second droplet is placed. For most experiments, droplets were digitally printed onto bare glass (microscope slides) with just one

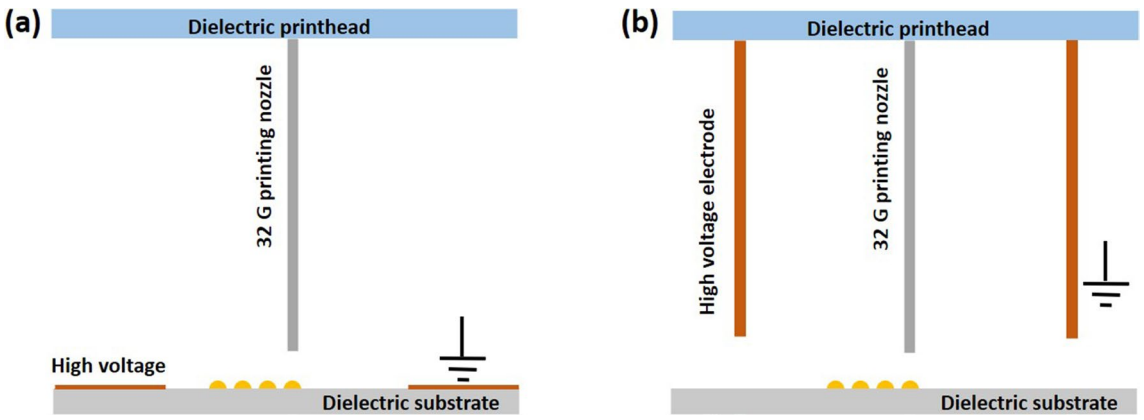

Fig. 1 Schematic of the experimental setups. **a** Horizontal electrodes on the dielectric substrate. **b** Vertical electrodes mounted on the printhead over the dielectric substrate

case being printed onto a glass slide covered with Mylar film. The Mylar film, a semi-transparent, flexible film served as a simple means to alter the hydrophilic nature of glass and diversify experiments.

For the initial experiment, several droplets of linseed oil were printed between two horizontal electrodes aligned on the surface of the glass substrate. The electrodes were made by applying self-adhesive copper tape to the glass microscope slide with an insulation gap of 3 cm in-between, as sketched in Fig. 1a. Initially, the droplets were in steady state, as shown in Fig. 2a. When the electric field had been applied, the droplets underwent stretching along the joint central line and coalesced into an intact line, as illustrated in the series of snapshots in Figs. 2b–e. A slight asymmetry was noticed relative to the center of the printing line both before and after electrocoalescence. While the former is due to fluctuations during flight and impact, the latter is likely due to asymmetry in the E.F. generated by the handmade electrodes, as well as the initial variances from droplet deposition. It should also be noted that this process worked equally well when Spot-E was chosen for the printing ink.

Figure 2 demonstrates the ability to redistribute fluid from individual droplets into a continuous trace line with the surface-aligned electrode configuration. To investigate the practically important electrode configuration of Fig. 1b, a dielectric printhead with copper electrodes (0.75 mm × 12 mm × 20 mm strips) parallel to the nozzle with an insulation gap of 5.08 cm was used. The dielectric printhead was made from 1.5 cm thick Teflon and modeled after the original aluminum printhead giving approximately 6 cm × 6 cm to mount the printing needle and electrodes. This modified printhead was retrofitted to the DIW automated dispensing robot and tested to ensure normal operation. Figure 3 shows a schematic time-lapse of the modified printing process. With the printing nozzle extending below the lowest end of the attached electrodes, the printer can run through a normal program as depicted in Fig. 3a. After printing the droplets for the desired trace, a simple modification to the program lowers the electrodes till they are just above the substrate (~1 mm) and centers them over above the print before applying high-voltage to create an E.F. strength of 1.57 kV/cm, as depicted in Fig. 3b. This E.F. strength was chosen based on experiments from previous work (Plog et al. 2019). When the E.F. strength was varied slightly for experimental purposes, the value of ~ 1.57 kV/cm (corresponding to the potential difference of 8 kV applied over the distance

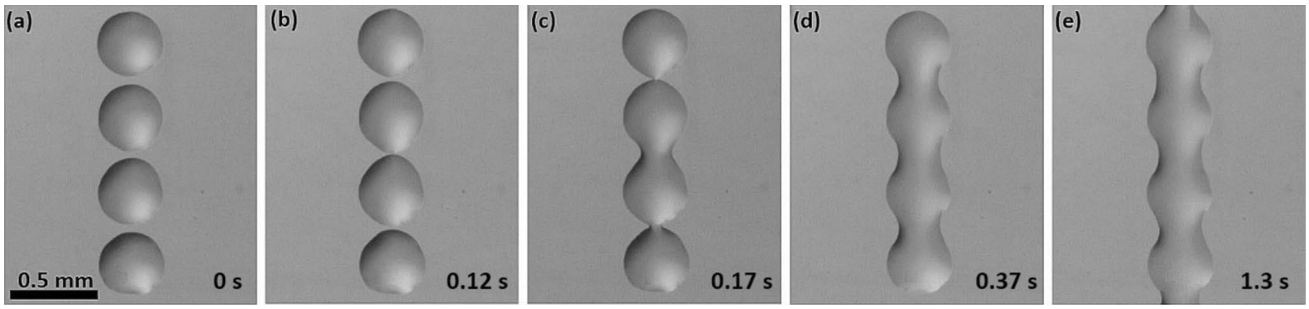

Fig. 2 Linseed oil on glass slide subjected to the electric field strength of 1.57 kV/cm. The surface-aligned electrode configuration of Fig. 1a

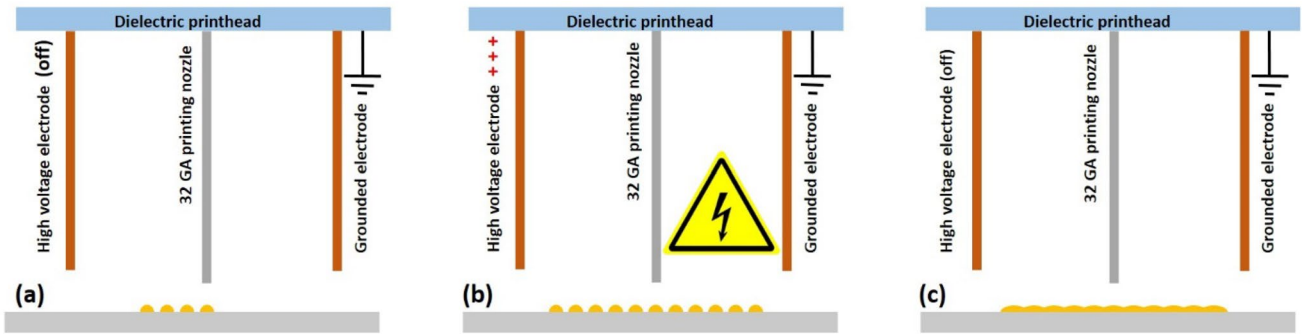

Fig. 3 Schematic of the experiment setup throughout notable positions of the print (not to scale). **a** Needle directly above digital location as the droplet is ejected. **b** While the needle is not printing, electrodes centered over the area of interest are charged to create the horizontal electric field strength of 1.57 kV/cm. Area of interest is tunable via electrode spacing; here it was 5.08 cm. **c** All printing motion and electrical processes have stopped; the finished line or trace having experienced the effect of the applied electric field and subsequently coalesced

of 5.08 cm) was found to be effective and used throughout experiments to maintain consistency. No better results were achieved when E.F. strength values were different. Figure 3c shows the DIW robot at idle, after the droplets have coalesced. In general, Fig. 3 sketches the time evolution of two coalescing droplets. The impulse causes a droplet deformation, which lowers the distance between them. Coalescence is triggered if the distance between the droplets is fully covered by deforming liquid surface. During coalescence the contact line of both droplets is pinned. After coalescence the contact line of the resulting droplet moves and the contact angle is changed.

Figure 4 shows the snapshots before and after the electrocoalescence process in several situations. First, linseed oil droplets were deposited (Fig. 4a1), and then subjected to the electric force resulting from the 1.57 kV/cm E.F. strength produced on the printhead. Figure 4a shows a clear separation between droplets ensuring a steady-state situation where coalescence is highly improbable corresponding to the schematic in Fig. 3a. The previous images (Fig. 2) captured by high-speed camera reveal stretching at each side of the droplet forming an appearance of a 'double cone') in alignment with the E.F strength vector. Unfortunately, this real-time top view was now being blocked by the printhead and inadmissible for recording during the printing process. Accordingly, the images in Fig. 4 are the static images taken before (e.g., Fig. 4a1) and after the entire process (the corresponding Fig. 4a2). In Figs. 4b1 and b2, Spot-E was the chosen ink and was printed on a Mylar substrate supported by glass. Through trial and error, an initial droplet spacing was chosen close to the threshold of self-coalescence. Being printed on the threshold of coalescence, Fig. 4b1 captures a case where the majority of the printed droplets having coalesced, leaving just one small break in the middle of the trace. To fix the broken line with the E.F. application, the modified printhead with electrodes was positioned over the break before charging to 1.57 kV/cm. As Fig. 4b2 shows, the E.F. can effectively repair a failed discontinuous print trace without any need to reprint.

It should be emphasized that the resulting printed geometry in Fig. 4a2 does not eliminate all budging which may be disadvantageous for some applications. In general, budging depends on the following four factors being at work simultaneously: (1) the initial waviness of the liquid front depending on the droplet size and the inter-droplet distance, (2) the surface wettability depending on the liquid and the solid substrate, (3) surface tension of the liquid, and (4) its viscous damping smoothing. Accordingly, it can be seen in Fig. 4b2 that in the second case the resulting trace has less budging than that in Fig. 4a2. It should be also noted that less overall material is used to create continuous traces with this technique, which is definitely beneficial for "green" printing applications. Also worth mentioning is the ability to tune the waviness of the trace line, and the surface roughness. Indeed, Fig. 5 highlights by red arrows the peaks of the printed line when viewing sideways on the horizontal printing plane. Looking back to Fig. 4a1, a distinct and repeatable distance between roughness peaks and troughs can be

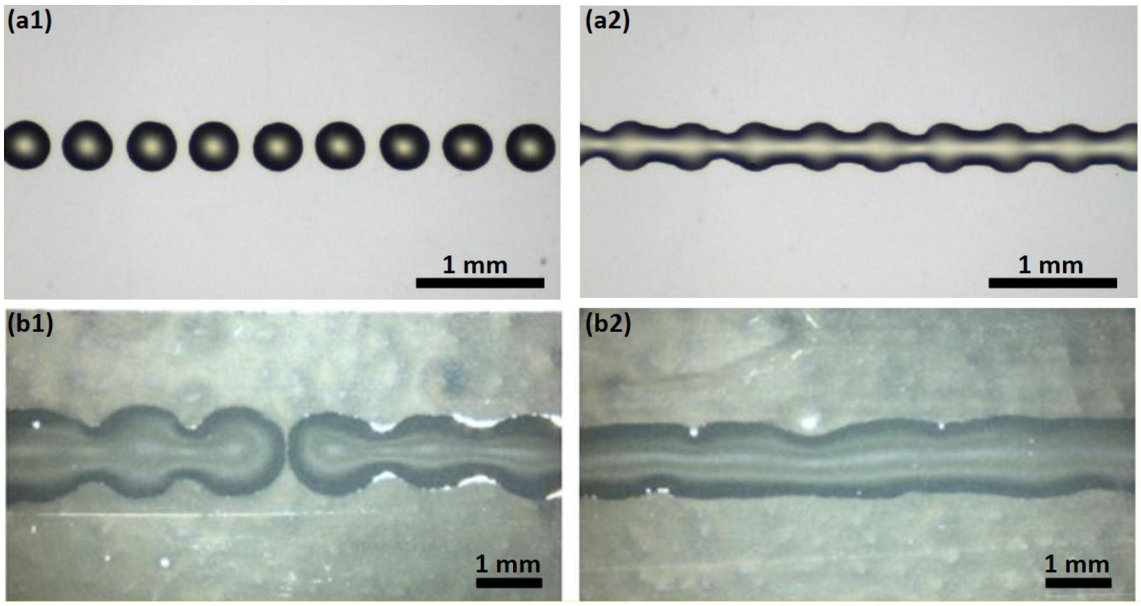

Fig. 4 Printed line with droplet of linseed oil on glass at spacing above the thresholds for self-coalescence: **a1** before applied E.F., **a2** after the E.F. strength of 1.57 kV/cm has been applied and droplet coalescence achieved. **b1** Spot-E printing on Mylar at the threshold of self-coalescence resulting in a randomly discontinuous trace. **b2** after the E.F. strength of 1.57 kV/cm has been applied, the results reveal a smoother continuous trace

achieved. Because the frequency of surface roughness is directly linked to the number of droplets over a given length, both adjusting the size of droplets and/or varying the spacing of droplets provides the ability to tune the waviness of the printed surface. As hydrophilicity/phobicity are known to vary with surface roughness at the micro-/nano-scales, the present results might be useful to change wettability and adhesive properties without chemical alteration.

A number of works related to applications of the inkjet techniques in printed electronics ascertain significant interest in printed thin films (Tong et al. 2018; Fukuda and Someya 2017; Lu et al. 2014; Boley et al. 2013; Ikegawa and Azuma 2004). With this in mind, the arrays of droplets shown in Fig. 6a1 and b1 were subjected to the same charged electrode configuration as that in Fig. 3b. The resulting liquid configurations after application of the E.F. shown in Fig. 6a2 and b2, respectively, reveal that the E.F. promotes film formation. While complete coalescence of all droplets into a thin film was not achieved in the present experiments yet, several domains in Figs. 6a2 and b2 do reveal uniform films, which clearly shows that formation of such films over large printed areas should be possible. For example, the ability to rotate or alter the E.F. lines may facilitate the overall droplet coalescence resulting in thin uniform films. Future work will explore whether additional electrodes or ring-like electrodes could facilitate formation of uniform films.

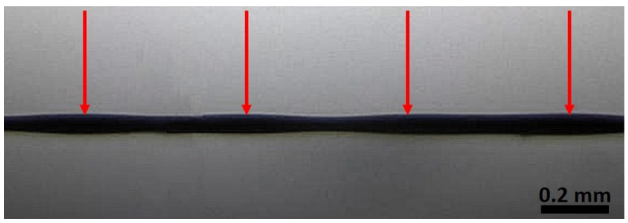

Fig. 5 Surface waviness of printed linseed oil with selective droplet spacing

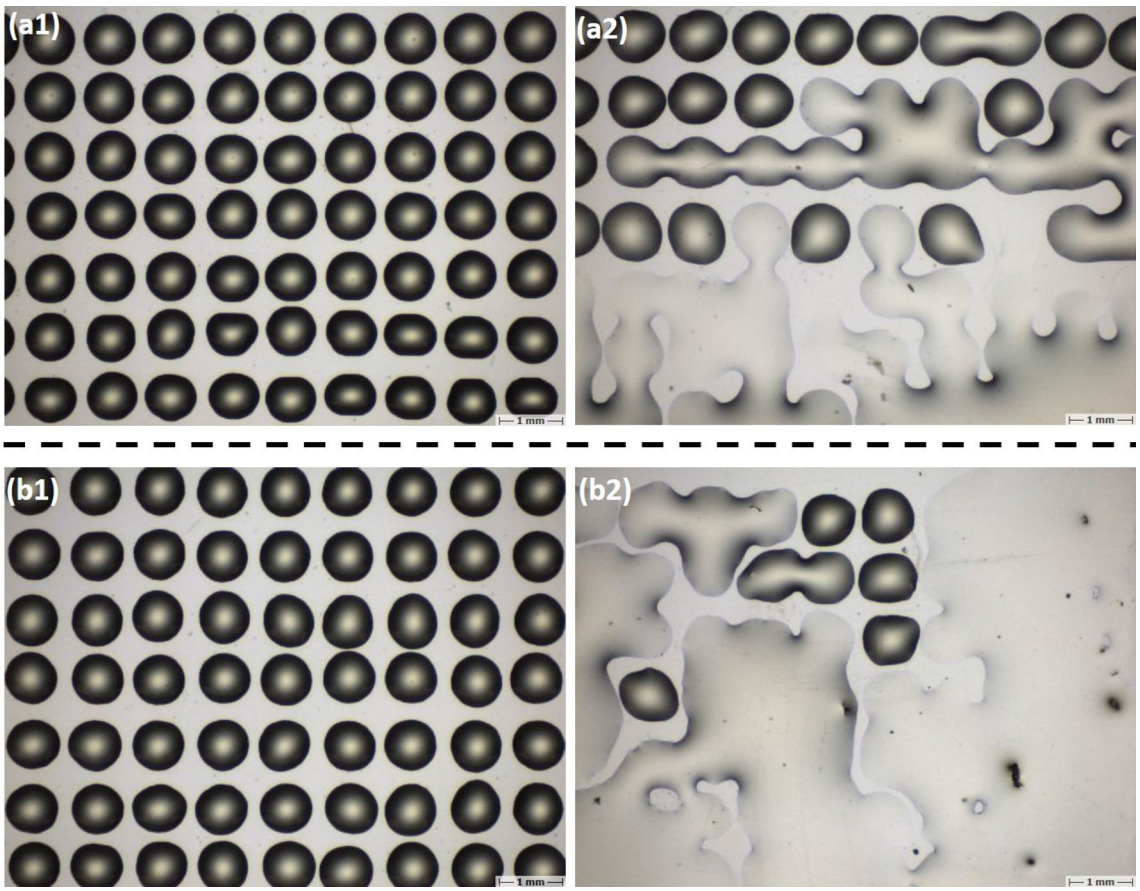

Fig. 6 Printed arrays of linseed oil on glass used for electrically driven film formation. **a1** Before the E.F. was applied (case 1), and **a2** the corresponding image after the E.F. has been applied in case 1. **b1** Before the E.F. was applied (case 2), and **b2** the corresponding image after the E.F. has been applied in case 2

3 Conclusion

The experimental results of the present research affirm that an electric field purposely created and oriented near a printing orifice can have a significant effect on droplet coalescence on the substrate. This electrically enhanced printing process offers the ability to control or tune printing parameters in 3D printing due to a greater window of droplet coalescence. The addition of an E.F. near the printing orifice allowed droplets to be printed with spacing much greater than those found in literature while still achieving an intact trace through coalescence. Potential advantages of this printing enhancement include: a reduced volume of ink, adjustable modulation of the printed surface roughness, reduced printing defects, and the ability to connect broken traces when a conventional printing method has failed. The Coulomb force employed here can be accurately controlled, is repeatable and easily scalable to industrial applications.

For the present work, a commercially available printer was modified with the inclusion of two electrodes equally distanced from the nozzle creating a controllable transverse electric field. Two inks including linseed oil and a photo-curable resin (Spot-E) were tested, and in both cases extended initial distances between droplets prior to their electrocoalescence were used. While the ability of the E.F. to coalesce lines into thin films was not as pronounced as in the experiments where droplets were combined into continuous lines, the present experiments reveal a proof of concept and prospective possibilities for thin film formation for jetting-based 3D printing of printed electronics. Since no electrodes are on or beneath the printing surface in the present case, the enhancements gained from the E.F. will remain consistent through a layer-by-layer build. Whether being implemented into new designs, or retrofitted onto existing, the present innovative technique holds great promise of transforming discreet droplet arrays into lines or thin films with tuneable parameters and versatility not found in conventional jetting-based printing.

Acknowledgements This work was supported by the National Science Foundation (NSF) Grant 1825626.

References

Andrieu C, Beysens D, Nikolayev V, Pomeau Y (2002) Coalescence of sessile drops. J Fluid Mech 453:427–438

Aydemir C, Karademir A, İmamoğlu S (2010) Effects of filler content and coating on the water and oil-based ink interactions with a paper surface. Int J Polym Mater 59:891–901

Aydemir C, Yenidoğan S, Karademir A, Arman Kandirmaz E (2018) The examination of vegetable-and mineral oil-based inks' effects on print quality: green printing effects with different oils. J Appl Biomater Funct Mater 16:137–143

Bhuvana T, Boley W, Radha B, Dolash BD, Chiu G, Bergstrom D, Kulkarni GU (2010) Inkjet printing of palladium alkanethiolates for facile fabrication of metal interconnects and surface-enhanced Raman scattering substrates. Micro Nano Lett 5:296–299

Boley JW, Shou C, McCarthy P, Fisher T, Chiu G (2013) The role of coalescence in inkjet printing functional films: an experimental study. Soc Imaging Sci Technol 2:508–513

Boley W, Bhuvana T, Hines B, Sayer RA, Chiu G, Fisher TS, Kulkarni GU (2009). Inkjet printing involving palladium alkanethiolates and carbon nanotubes functionalized with single-strand DNA. In: NIP and Digital Fabrication Conference, Soc. Imaging Sci Technol, vol 2, pp 824–827

Castellanos A, Pérez A (2007) Electrohydrodynamic systems. In: Tropea C, Yarin AL, Foss J (eds) Springer handbook of experimental fluid mechanics. Springer, Heidelberg, pp 1317–1333

Castrejon-Pita JR, Betton ES, Kubiak KJ, Wilson MCT, Hutchings IM (2011) The dynamics of the impact and coalescence of droplets on a solid surface. Biomicrofluidics 5:014112

Chang H-C, Yeo LY (2010) Electrokinetically driven microfluidics and nanofluidics. Cambridge University Press, Cambridge

Cho SK, Moon H, Kim C (2003) Creating, transporting, cutting, and merging liquid droplets by electrowetting-based actuation for digital microfluidic circuits. J Microelectromech Syst 12:70–80

De Gans BJ, Duineveld PC, Schubert US (2004) Inkjet printing of polymers: state of the art and future developments. Adv Mater 16:203–213

Duineveld PC (2003) The stability of ink-jet printed lines of liquid with zero receding contact angle on a homogeneous substrate. J Fluid Mech 477:175–200

Fidalgo LM, Whyte G, Bratton D, Kaminski CF, Abell C, Huck WT (2008) From microdroplets to microfluidics: selective emulsion separation in microfluidic devices. Angeur Chem Int Ed 47:2042–2045

Franke T, Abate AR, Weitz DA, Wixforth A (2009) Surface acoustic wave (SAW) directed droplet flow in microfluidics for PDMS devices. Lab Chip 9:2625–2627

Fukuda K, Someya T (2017) Recent progress in the development of printed thin-film transistors and circuits with high-resolution printing technology. Adv Mater 29:1602736

Gokhale SJ, DasGupta S, Plawsky JL, Wayner PC (2004) Reflectivity-based evaluation of the coalescence of two condensing drops and shape evolution of the coalesced drop. Phys Rev E 70:051610

Hung LH, Choi KM, Tseng WY, Tan YC, Shea K, Lee AP (2006) Alternating droplet generation and controlled dynamic droplet fusion in microfluidic device for CdS nanoparticle synthesis. Lab Chip 6:174–178

Ikegawa M, Azuma H (2004) Droplet behaviors on substrates in thin-film formation using ink-jet printing. JSME Int J Ser B 47:490–496

Koivula H (2012) Studies in offset ink setting. Doctoral Thesis, Akadeni University

Kumar V, Boley JW, Yang Y, Ekowaluyo H, Miller JK, Chiu GTC, Rhoads JF (2011) Bifurcation-based mass sensing using piezoelectrically-actuated microcantilevers. Appl Phys Lett 98:153510

Landau LD, Lifshitz EM (1987) Fluid mechanics, 2nd edn. Pergamon, New York

Lee MW, Kang DK, Yoon SS, Yarin AL (2012) Coalescence of two drops on partially wettable substrates. Langmuir 28:3791–3798

Lee MW, Latthe S, Yarin AL, Yoon SS (2013) Dynamic electrowetting-on-dielectric (DEWOD) on unstretched and stretched Teflon. Langmuir 29:7758–7767

Li R, Ashgriz N, Chandra S, Andrews JR, Drappel S (2010) Coalescence of two droplets impacting a solid surface. Exp Fluids 48:1025–1035

Link D, Anna SL, Weitz DA, Stone H (2004) Geometrically mediated breakup of drops in microfluidic devices. Phys Rev Lett 92:54503
Löwe JM, Hinrichsen V, Tropea C (2018). Droplet behavior under the impact of lightning and switching impulse voltage. In 2018 IEEE Electrical Insulation Conference (EIC) 443–447. IEEE
Lu Z, Layani M, Zhao X, Tan LP, Sun T, Fan S, Hng H (2014) Fabrication of flexible thermoelectric thin film devices by inkjet printing. Small 10:3551–3554
Maddaus A, Curley P, Griswold MA, Costa BD, Hou S, Jeong KJ, Deravi LF (2016) Design and fabrication of bio-hybrid materials using inkjet printing. Biointerphases 11:041002
Matavž A, Malič B (2018) Inkjet printing of functional oxide nanostructures from solution-based inks. J Sol-Gel Sci Technol 87:1–21
Melcher JR, Taylor GI (1969) Electrohydrodynamics: a review of the role of interfacial shear stresses. Annu Rev Fluid Mech 1:111–146
Nardes AM, Kemerink M, Janssen RA, Bastiaansen JA, Kiggen NM, Langeveld BM, De Kok M (2007) Microscopic understanding of the anisotropic conductivity of PEDOT: PSS thin films. Adv Mater 19:1196–1200
Nguyen NT, Ting TH, Yap YF, Wong TN, Chai J, Ong W, Zhou J, Tan S, Yobas L (2007) Thermally mediated droplet formation in microchannels. Appl Phys Lett 91:084102–084103
Ozkan M, Wang M, Ozkan C, Flynn R, Esener S (2003) Optical manipulation of objects and biological cells in microfluidic devices. Biomed Microdevice 5:61–67
Plog J, Löwe JM, Jiang Y, Pan Y, Yarin AL (2019) Control of direct written ink droplets using electrowetting. Langmuir 35:11023–11036
Plog J, Jiang Y, Pan Y, Yarin AL (2020a) Electrostatic charging and deflection of droplets for drop-on-demand 3D printing within confinements. Addit Manuf 36:101400
Plog J, Jiang Y, Pan Y, Yarin AL (2020b) Electrostatically-assisted direct ink writing for additive manufacturing. Addit Manuf. https://doi.org/10.1016/j.addma.2020.101644
Rayleigh L (1896) The theory of sound, vol 2. Macmillan, New York
Russel WB, Saville DA, Schowalter WR (1992) Colloidal Dispersions. Cambridge University Press, Cambridge
Salaoru I, Maswoud S, Paul S (2019) Inkjet printing of functional electronic memory cells: a step forward to green electronics. Micromachines 10:417
Samoska LA (2011) An overview of solid-state integrated circuit amplifiers in the submillimeter-wave and THz regime. IEEE Trans Terahertz Sci Technol 1:9–24
Sarojini KGK, Dhar P, Varughese S, Das SK (2016) Coalescence dynamics of PEDOT: PSS droplets impacting at offset on substrates for inkjet printing. Langmuir 32:5838–5851
Saville DA (1997) Electrohydrodynamics: the Taylor-Melcher leaky dielectric model. Annu Rev Fluid Mech 29:27–64
Seipel S, Yu J, Periyasamy AP, Viková M, Vik M, Nierstrasz VA (2018) Inkjet printing and UV-LED curing of photochromic dyes for functional and smart textile applications. RSC Adv 8:28395–28404
Shimoda T, Morii K, Seki S, Kiguchi H (2003) Inkjet printing of light-emitting polymer displays. MRS Bull 28:821–827
Singh M, Haverinen HM, Dhagat P, Jabbour GE (2010) Inkjet printing—process and its applications. Adv Mater 22:673–685
Soltman D, Smith B, Kang H, Morris SJS, Subramanian V (2010) Methodology for inkjet printing of partially wetting films. Langmuir 26:15686–15693
Stringer J, Derby B (2010) Formation and stability of lines produced by inkjet printing. Langmuir 26:10365–10372
Tong S, Sun J, Yang J (2018) Printed thin-film transistors: research from China. ACS Appl Mater Interfaces 10:25902–25924
Vaithilingam J, Saleh E, Wildman RD, Hague RJ, Tuck CJ (2018) Optimisation of substrate angles for multi-material and multi-functional inkjet printing. Sci Rep 8:1–8
Wang W, Yang C, Li CM (2009) On-demand microfluidic droplet trapping and fusion for on-chip static droplet assays. Lab Chip 9:1504–1506
Wu JT, Hsu SLC, Tsai MH, Liu YF, Hwang WS (2012) Direct ink-jet printing of silver nitrate–silver nanowire hybrid inks to fabricate silver conductive lines. J Mater Chem 22:15599–15605
Yarin AL, Pourdeyhimi B, Ramakrishna S (2014) Fundamentals and applications of micro- and nanofibers. Cambridge University Press, Cambridge
Zeng S, Li B, Su X, Qin J, Lin B (2009) Microvalve-actuated precise control of individual droplets in microfluidic devices. Lab Chip 9:1340–1343
Zhao L, Pan L, Zhang K, Guo S, Liu W, Wang Y, Chen Y, Zhao X, Chan H (2009) Generation of Janus alginate hydrogel particles with magnetic anisotropy for cell encapsulation. Lab Chip 9:2981–2986